Comprehensive Profiling of Poor-Risk Paired Primary and Recurrent Triple-Negative Breast Cancers Reveals Immune Phenotype Shifts

Katherine E. Hutchinson[1], Susan E. Yost[2], Ching-Wei Chang[3], Radia Marie Johnson[4], Adrian R. Carr[5], Paul R. McAdam[5], Daniel L. Halligan[5], Chun-Chieh Chang[3], Daniel Schmolze[6], Jackson Liang[1], and Yuan Yuan[2]

ABSTRACT

Purpose: Emerging data suggest immune checkpoint inhibitors have reduced efficacy in heavily pretreated triple-negative breast cancers (TNBC), but underlying mechanisms are poorly understood. To better understand the phenotypic evolution of TNBCs, we studied the genomic and transcriptomic profiles of paired tumors from patients with TNBC.

Experimental Design: We collected paired primary and metastatic TNBC specimens from 43 patients and performed targeted exome sequencing and whole-transcriptome sequencing. From these efforts, we ascertained somatic mutation profiles, tumor mutational burden (TMB), TNBC molecular subtypes, and immune-related gene expression patterns. Stromal tumor-infiltrating lymphocytes (stromal TIL), recurrence-free survival, and overall survival were also analyzed.

Results: We observed a typical TNBC mutational landscape with minimal shifts in copy number or TMB over time. However, there were notable TNBC molecular subtype shifts, including increases in the Lehmann/Pietenpol-defined basal-like 1 (BL1, 11.4%–22.6%) and mesenchymal (M, 11.4%–22.6%) phenotypes, and a decrease in the immunomodulatory phenotype (IM, 31.4%–3.2%). The Burstein-defined basal-like immune-activated phenotype was also decreased (BLIA, 42.2%–17.2%). Among downregulated genes from metastases, we saw enrichment of immune-related Kyoto Encyclopedia of Genes and Genomes pathways and gene ontology (GO) terms, and decreased expression of immunomodulatory gene signatures ($P < 0.03$) and percent stromal TILs ($P = 0.03$). There was no clear association between stromal TILs and survival.

Conclusions: We observed few mutational shifts, but largely consistent transcriptomic shifts in longitudinally paired TNBCs. Transcriptomic and IHC analyses revealed significantly reduced immune-activating gene expression signatures and TILs in recurrent TNBCs. These data may explain the observed lack of efficacy of immunotherapeutic agents in heavily pretreated TNBCs. Further studies are ongoing to better understand these initial observations.

See related commentary by Savas and Loi, p. 526

Introduction

Triple-negative breast cancer (TNBC) represents approximately 15% of breast cancers and is characterized by the lack of expression of estrogen receptor (ER), progesterone receptor (PR), and HER2 (1). Despite recent FDA approval of atezolizumab for the first-line treatment of TNBC (2), the current standard-of-care treatment for TNBC is still cytotoxic chemotherapy, and the only FDA-approved targeted therapies are the PARP inhibitors olaparib and talazoparib for *BRCA1/2*-mutant TNBCs (3, 4). Regardless of early aggressive chemotherapy, the lack of effective targeted therapies in the advanced setting lends an overall poor prognosis for patients with TNBC (5).

TNBC is clinically aggressive, with a high degree of chromosomal instability and extensive inter- and intratumoral heterogeneity (6, 7). Differential gene expression profiling enables subclassification of TNBCs into several molecular subtypes, the most commonly recognized of which are the Lehmann–Pietenpol (8) and Burstein (9) classification systems. In the former, TNBCs are molecularly grouped into six subtypes: basal-like 1 (BL1), basal-like 2 (BL2), immunomodulatory (IM), mesenchymal (M), mesenchymal stem-like (MSL), and luminal androgen receptor (LAR; ref. 8). In a recent update, these subtypes have been revised and limited to four subtypes: BL1, BL2, M, and LAR (10). Similarly, Burstein and colleagues described four subtypes: LAR, mesenchymal (MES), basal-like/immune suppressed (BLIS), and basal-like/immune-activated (BLIA; ref. 9). In addition to tumor heterogeneity, acquired genetic subclones resulting from chemotherapy selection pressure may lead to treatment resistance (11–13).

With the development of large-scale molecular profiling technologies, understanding of the TNBC genomic landscape has improved, but currently available datasets from Molecular Taxonomy of Breast Cancer International Consortium (14) and The Cancer Genome Atlas (TCGA; ref. 15) are limited to primary, treatment-naïve breast cancers only. In-depth molecular analyses of metastatic TNBC compared with paired primary specimens are required to inform molecular changes as a result of chemotherapy selection pressure. Previous studies were limited by their sample size, and the findings remain inconclusive (16).

Immune checkpoint inhibitors (ICI) have been under rigorous investigation in multiple TNBC clinical studies (2, 17–21). Recent results from IMpassion130 showed a promising response rate of 56%

[1]Oncology Biomarker Development, Genentech, Inc., South San Francisco, California. [2]Department of Medical Oncology and Therapeutic Research, City of Hope National Medical Center, Duarte, California. [3]Oncology Biostatistics, Genentech, Inc., South San Francisco, California. [4]Oncology Bioinformatics, Genentech, Inc., South San Francisco, California. [5]Fios Genomics, Edinburgh, United Kingdom. [6]Department of Pathology, City of Hope National Medical Center, Duarte, California.

Note: Supplementary data for this article are available at Clinical Cancer Research Online (http://clincancerres.aacrjournals.org/).

Corresponding Author: Yuan Yuan, City of Hope National Medical Center, 1500 E. Duarte Road, Duarte, CA 91010. Phone: 626-471-9200; Fax: 626-301-8233; E-mail: yuyuan@coh.org

Clin Cancer Res 2020;26:657–68

doi: 10.1158/1078-0432.CCR-19-1773

Translational Relevance

The molecular heterogeneity of triple-negative breast cancers (TNBC) lends difficulty in identifying effective targeted therapies against TNBC. Atezolizumab was recently approved for the treatment of PD-L1–positive, unresectable locally advanced, or metastatic TNBC in combination with protein-bound paclitaxel. Results from recent clinical trials, however, suggest immune checkpoint inhibitors have reduced efficacy in heavily pretreated, and presumably, more heterogeneous TNBCs. The work described herein suggests that in the transition from primary to metastatic disease, TNBCs treated with traditional chemotherapy regimens exhibit decreased immune activity over time. This is illustrated by decreased stromal tumor-infiltrating lymphocytes and decreased expression of immune activity–related gene signatures in metastatic TNBCs. These phenotypes may partially explain the limited efficacy of immune checkpoint inhibitors in the metastatic setting and highlight the importance of their use instead in the early neoadjuvant setting.

when atezolizumab was combined with nab-paclitaxel compared with 45.9% in patients with TNBC treated first-line with nab-paclitaxel alone (2). In the neoadjuvant ISPY-2 study, adding pembrolizumab to a paclitaxel, adriamycin, and cyclophosphamide regimen increased the complete pathologic response rate (pCR) from approximately 20% to 62% ($n = 21$; ref. 21). However, the efficacy of ICIs varies significantly depending on the line of therapy. For example, single-agent checkpoint inhibition elicits a much lower response rate (5%–6%) in the late-line setting compared with response rates of 19% to 24% when administered as first-line treatment (17–20). These emerging clinical data suggest checkpoint inhibition is less effective in heavily pretreated TNBCs, but the underlying mechanisms are not well understood. To investigate the immuno-phenotypic evolution of TNBC, we studied the genomic and transcriptomic profiles of tumors from patients undergoing treatment for TNBC.

Materials and Methods

Patient selection, ethical approval, and consent to participate

Paired TNBC specimens were identified through a City of Hope (COH) Institutional Review Board (IRB)–approved retrospective protocol (IRB 07047) via the COH Biorepository from patients with breast cancer treated at COH from 2002 to 2015. Eligible patients had the following features: TNBC with recurrence; at least one tumor biospecimen available from initial surgery or biopsy; at least one specimen available from relapsed disease biopsy; and clinical outcomes data. All collected samples were formalin-fixed paraffin-embedded (FFPE).

Histologic assessments

Histopathology of specimens was obtained from original pathology reports after being reviewed by two independent pathologists. ER, PR, and HER2 status were determined using standard American Society of Clinical Oncology/College of American Pathologists guidelines. Immune cell subset profile changes were analyzed by TIL quantification of hematoxylin and eosin–stained slides, according to the International Immuno-Oncology Biomarker Working Group on Breast Cancer Guidelines (22).

Clinicopathologic analysis

Patient characteristics were obtained via chart review. Demographic data including age, gender, date of birth, date of diagnosis, date of relapse, and date of death (if applicable) were obtained. Tumor characteristics including tumor size, histology type, grade, lymph node involvement, and treatment variables including chemotherapy were also obtained. Clinical outcomes including overall survival (OS), relapse-free survival (RFS), survival after relapse (SAR), and time between specimen collections (TBC) were also calculated. OS was defined as the date of surgery to date of death. RFS was defined as date of surgery to date of first relapse. SAR was defined as the date of relapse to the date of death. TBC was defined as the difference in time between the date of collection of the first specimen of a pair and the second specimen of a pair. Per physician decision, in the neoadjuvant or adjuvant setting (termed "adjuvant/neoadjuvant" herein), patients received either no chemotherapy or one of the following regimens: Adriamycin-containing, platinum-containing, Adriamycin+platinum, or taxane-containing.

Targeted next-generation sequencing (FoundationOne)

Genomic alterations in FFPE specimens from primary and recurrent TNBCs were detected using the FoundationOne targeted next-generation sequencing (NGS) panel at a Clinical Laboratory Improvement Amendments–certified, College of American Pathologists-accredited reference laboratory (Foundation Medicine, Inc.). FoundationOne identifies base substitutions, insertions and deletions, amplifications with copy number $\geq$6, and rearrangements. More comprehensive details on the FoundationOne platform version, sequencing, and mutation calling methodologies can be found in the Supplementary Data.

Whole-transcriptome sequencing (RNA sequencing)

Sequencing libraries were generated using the Illumina TruSeq RNA Access method, a hybridization-based protocol to enrich for coding RNAs from total RNA sequencing (RNA-seq) libraries. The method consists of two major steps: total RNA library preparation and coding RNA library enrichment. First-strand cDNA synthesis is primed from total RNA using random primers, followed by the generation of second-strand cDNA with dUTP (in place of dTTP) in the master mix. This facilitates the preservation of strand information, as amplification in subsequent steps will stall when it encounters Uracil in the nucleotide strand. Double-stranded cDNA undergoes end-repair, A-tailing, and ligation of adapters that include index sequences. The resulting molecules are amplified via PCR, their yield and size distribution are determined using a BioAnalyzer, and their concentrations are normalized in preparation for the enrichment step. Libraries are enriched for the mRNA fraction by positive selection using a cocktail of biotinylated oligos corresponding to coding regions of the genome. Targeted library molecules are then captured through the hybridized biotinylated oligo probe using streptavidin-conjugated beads. After two rounds of hybridization/capture reactions, the enriched library molecules are PCR amplified, quantified, then normalized and pooled in preparation for sequencing. Please refer to the Supplement for comprehensive details on the methodologies for whole-transcriptome data processing and data normalization.

Gene expression and pathway analyses

Differential gene expression was evaluated by applying an empirical Bayesian approach, using paired expression data from primary and

metastatic samples for each patient. At the standard statistical threshold (FDR-adjusted P value < 0.05), a total of 1,011 genes were significantly differentially expressed. In addition, continuous Cox proportional hazards regression models were fit to the data to investigate the impact of individual gene expression on OS, RFS, SAR, and TBC. In a Cox regression analysis, the effect of a predictor variable (e.g., the expression level of a gene) on the relative likelihood of an event (e.g., death or relapse) occurring at any given point in time can be expressed as the HR. The HR value represents the predicted increase or decrease in this likelihood for a unit increase in the predictor. Hence, genes which are assigned HR values > 1 are associated with increased hazard rates (i.e., shorter time to event when the gene is more highly expressed), whereas those assigned HR values <1 are associated with decreased hazard rates (i.e., longer time to event when the gene is more highly expressed). At an FDR-adjusted P value <0.05, few features had significant HRs in the Cox regression analyses; therefore, a less stringent threshold of raw (unadjusted) P value < 0.01 was used for comparisons.

Significant genes (raw P value < 0.01) from each contrast were analyzed for significant enrichment of Kyoto Encyclopedia of Genes and Genomes (KEGG) pathway membership and for GO terms across all three gene ontologies using a hypergeometric test. The resulting P value was then corrected for tests over multiple KEGG pathways or GO terms using the method of Benjamini and Hochberg (1995) to yield an adjusted P value. Enrichment (P < 0.01) was assessed for up- and downregulated genes separately.

Gene set enrichment analyses

For enrichment analyses, genes were ranked based on the P value of differential expression. Specifically, $\log_{10}(P$ value) was used to rank genes, with negative/positive values used for downregulated/upregulated genes, respectively. This ranked list was then used in Gene Set Enrichment Analysis (GSEA), as implemented by fgsea (23), to search for enrichment of KEGG pathway and GO term membership (across all three gene ontologies). The resulting P values were corrected for tests over multiple KEGG pathways or GO terms using the method of Benjamini and Hochberg (1995) to yield an adjusted P value.

Breast cancer molecular subtyping

The prediction of PAM50 subtype was based on a random-forest–based classifier that was developed from the RNA-seq data in TCGA (6) and 50 genes from the public PAM50 signature (24–26). Ninety-four randomly selected breast cancer samples from TCGA were used as an independent testing set, and the remaining samples were used to train the classifier. The Lehmann/Pietenpol classifier (8) was also trained by RNA-seq data from TCGA with the subtype call from available microarray data. The subtype call from microarray was treated as the "true" label, and a nearest-centroid–based classifier was developed. The classifier was then applied to the rest of TCGA samples without a microarray-based subtype call, and the performance was evaluated based on consensus clustering using all samples. The Burstein subtype classifier (9) was first evaluated using TNBC samples from TCGA with both available microarray and RNA-seq data. Nonnegative matrix factorization (NMF), a commonly used group of multivariate analysis algorithms used to cluster gene expression, was applied to both the microarray and RNA-seq data to determine the gene and sample groups. Due to the high concordance of subtype calls by the 80 genes in the Burstein classifier across the microarray and RNA-seq data (93%), we decided to directly use the 80 genes in the RNA-seq data without further feature selection. The groups of 80 genes were then further evaluated in an independent training set of 215 TNBC samples from two historical clinical trials (NCT01375842 and NCT02162719), and a random-forest–based classifier was trained with subtypes assigned by NMF. The classifier was implemented with an estimated "out-of-bag" error rate of 10%. The classifier was subsequently tested in an independent cohort of 51 TNBC samples from a third historical clinical trial (NCT02322814), and the NMF sample cluster result was ultimately considered as the label to evaluate performance.

Immune gene signature scoring

The immune gene signatures (gene lists) profiled in this study can be found in Supplementary Table S1. The composite score for the immune-activating genes ($n = 7$) from Denkert and colleagues (27) was defined as the median $\log_{10}$(CPM) expression of the indicated genes. From Ayers and colleagues (28), two gene expression signatures (lists) were analyzed: an 18-gene T-cell–inflamed signature and a 28-gene IFNγ signature. As a result of RNA-seq data processing and normalization procedures, the genes *HLA-DRA* and *HLA-E* were missing from the data and could not be analyzed in these two signatures. As such, scores for these two signatures were calculated based on the median $\log_{10}$(CPM) expression of the remaining genes in each signature. The score for the Th1 response–activating gene signature (29–31) was calculated as the median $\log_{10}$(CPM) expression of the genes contained in the signature.

xCell immune cell subtype deconvolution analysis

The normalized RNA-seq dataset was used to estimate cell subtypes using xCell (32) as implemented in the immunedeconv R package (33). Cell subtype proportions for each sample were summarized across the primary and metastatic samples and depicted as percentages in the heatmaps. Differences in proportions between the primary and metastatic groups were tested using a Wilcoxon signed rank test for each cell subtype, with P values adjusted for multiple test inflation using Benjamini–Hochberg correction (Supplementary Table S2).

Survival analysis

To investigate the relationship between tumor-infiltrating lymphocytes (% stromal TIL) with survival (OS and RFS), Cox proportional hazard models were fit separately for primary and metastatic samples. Categorical classification of % stromal TILs (<30% as "TIL-low" and ≥30% as "TIL-high") was used as the predictor variables in the survival analyses. HRs were generated as in the above Materials and Methods section titled "Gene Expression and Pathway Analyses," and survival curves were generated using the Kaplan–Meier method.

Other statistical analyses

For all statistical analyses not listed in Materials and Methods sections above, specific methods are delineated in the text and/or figure legends.

Ethical approval and consent to participate

All procedures performed in studies involving human participants were in accordance with the ethical standards of the institutional and/or national research committee and with the 1964 Helsinki Declaration and its later amendments or comparable ethical standards. All tumor specimens were identified through a COH IRB-approved retrospective protocol from patients consented to COH Biorepository Protocol IRB 07047. Informed consent was obtained from all of the participants of this study.

Table 1. Summary of patient characteristics.

Age ($n = 54$)	Years
Range	34–86
Median	51
Tumor histology ($n = 54$)	*N* (%)
Invasive ductal carcinoma	51 (94.4)
Invasive lobular carcinoma	2 (3.7)
Metaplastic	1 (1.9)
Clinical staging ($n = 54$)	*N* (%)
I	5 (9.3)
II	28 (51.9)
III	18 (33.3)
IV	3 (5.5)
Primary/metastatic pairs ($n = 43$)[a]	*N* (%)
Breast	10 (23.3)
Lymph node	7 (16.3)
Brain	7 (16.3)
Skin	6 (13.9)
Bone	4 (9.3)
Other sites[b]	9 (20.9)
Adjuvant/neoadjuvant chemotherapy ($n = 54$)[c]	*N* (%)
Adriamycin-containing	33 (61.1)
Platinum-containing	1 (1.9%)
Adriamycin + platinum	1 (1.9)
Taxane-containing	12 (22.2)
No chemotherapy	7 (12.9)
RFS ($n = 54$)	*N* (%)
<36 months	38 (70.4)
36–60 months	9 (16.7)
>60 months	7 (12.9)
OS ($n = 54$)	*N* (%)
<36 months	18 (33.3)
36–60 months	14 (25.9)
>60 months	13 (24.1)
Under active treatment	7 (13.0)
Lost to follow-up	2 (3.7)

[a]Eleven paired samples were longitudinal metastatic pairs.
[b]Other sites included ovary (2), pleural effusion (2), liver (1), muscle mass (1), adrenal gland (1), pericardium (1), and chest wall (1).
[c]Chemotherapy regimen listed was administered either as neoadjuvant or adjuvant treatment, per physician decision.

Results

Summary of clinical characteristics

Patient characteristics including histopathology, clinical staging, metastasis patterns, adjuvant/neoadjuvant chemotherapy, RFS, and OS are summarized in **Table 1**. Paired TNBC specimens from a total of 54 patients were analyzed, including 43 (79.6%) primary-metastatic (PM) pairs and 11 (20.4%) metastatic-metastatic (MM) pairs. Fifty-one (94.4%) patients had invasive ductal carcinoma, and 28 (51.9%) were stage II. Of the 43 paired PM samples, sites of metastases studied were: breast ($n = 10$, 23.3%); lymph node ($n = 7$, 16.3%), brain ($n = 7$, 16.3%), skin ($n = 6$, 13.9%), bone ($n = 4$, 9.3%), and other ($n = 9$, 20.9%). All but 7 patients received a chemotherapy-based treatment regimen. The most common regimen included adriamycin with ($n = 1$, 1.9%) or without ($n = 33$, 61.1%) a platinum agent. Twelve (22.2%) patients received a taxane-based regimen. The majority ($n = 37$, 68.5%) of patients in the cohort recurred within 36 months (**Table 1**).

Genomic landscape of TNBC from primary to metastatic disease

Thirty-four PM TNBC pairs (68 specimens) were successfully sequenced using the FoundationOne targeted NGS assay (**Fig. 1**; Supplementary Fig. S1). The most commonly observed genomic mutations were consistent with previously reported TNBC genomics (15). Of 34 paired primary and metastatic specimens, respectively, *TP53* was mutated in 29 (85.3%) and 30 (88.2%) tumors; *MYC* was mutated in 7 (20.6%) and 9 (26.5%); *PIK3CA* was mutated in 6 (17.6%) and 7 (20.6%); and *PTEN* alterations were observed in 6 (17.6%) and 6 (17.6%; **Fig. 1A**). **Figure 1A** only displays known oncogenic variants, per Foundation Medicine, Inc., curation (see Materials and Methods). As such, variants of unknown significance (VUS, Supplementary Fig. S2A–S2C), inclusive of many *BRCA1/2* variants, are not visible on the plot in **Fig. 1A**. *BRCA1* was mutated in 2 (5.9%) and 2 (5.9%); *BRCA2* was mutated in 6 (17.6%) and 6 (17.6%). Of note, both the primary and metastatic specimens from 2 patients exhibited amplifications of *CCND1* and *FGFs 3, 4*, and *19*, which is typically observed in 30% to 40% of hormone receptor–positive breast cancers (34, 35). The remaining observed mutations occurred sporadically throughout the cohort.

Although the individual frequency of shared and unique mutations between PM TNBC pairs may have varied by patient (**Fig. 1B** and **C**), overall 50% or more of mutations were shared between PM TNBC pairs. Specifically, of mutations annotated to be of known/likely oncogenic significance, 50% ($n = 123$) were shared between pairs, 16.3% ($n = 40$) were unique to primary TNBC specimens, and 33.7% ($n = 83$) were unique to metastatic triple-negative breast cancer (mTNBC) specimens (**Fig. 1B** and **C**). When VUSs were considered, 56.8% of mutations ($n = 536$) were shared, 12.1% ($n = 114$) were unique to primary specimens, and 31.1% ($n = 294$) were unique to metastatic specimens (Supplementary Fig. S2B and S2C). Overall, the mutational differences appear largely sporadic and are not consistent with a given gene or pathway (Supplementary Fig. S2D).

Similar to the mutational landscape, very few copy-number changes were observed in the transition from primary to metastatic disease (Supplementary Fig. S2E). Finally, tumor mutational burden (TMB) was less than 16 mutations per megabase (mut/Mb; **Fig. 1D**, TMB > 16 in one primary tumor and one metastatic tumor from different pairs), and no significant changes in TMB were observed between primary and metastatic TNBC pairs.

Breast cancer molecular subtype shifts between primary and metastatic disease

To understand the transcriptomic features of our TNBC cohort, we performed whole-transcriptome sequencing (RNA-seq) on PM pairs from 35 patients (70 specimens; Supplementary Fig. S1). Intrinsic breast cancer subtype phenotyping by PAM50 analysis (36–38) confirmed that 88.9% of primary samples were basal-like and remained basal-like (87.5%) through the transition to recurrent disease (Supplementary Fig. S3).

Previous microarray and whole-transcriptome breast cancer studies have led to the generation of TNBC molecular subtype classifiers. These include the six-subtype Lehmann/Pietenpol classifier (BL1, BL2, IM, M, MSL, and LAR; ref. 8) and the four-subtype Burstein classifier (LAR, MES, mesenchymal; BLIS, BLIA; ref. 9). Similar to the PAM50 analysis above, we used both the Lehmann/Pietenpol and Burstein molecular subtype classification systems to characterize the tumors in our dataset and to observe any shifts in these molecular phenotypes from primary to metastatic disease (see Materials and Methods). From the Lehmann/Pietenpol system, we observed an increase in tumors defined as BL1 (11.4% to 22.6%), an increase in tumors defined as mesenchymal (M, 11.4% to 19.4%), and a drastic decrease in tumors defined as IM (31.4% to 3.2%) from primary to metastatic tumors (**Fig. 2A**). Similarly, using the Burstein classification system, we

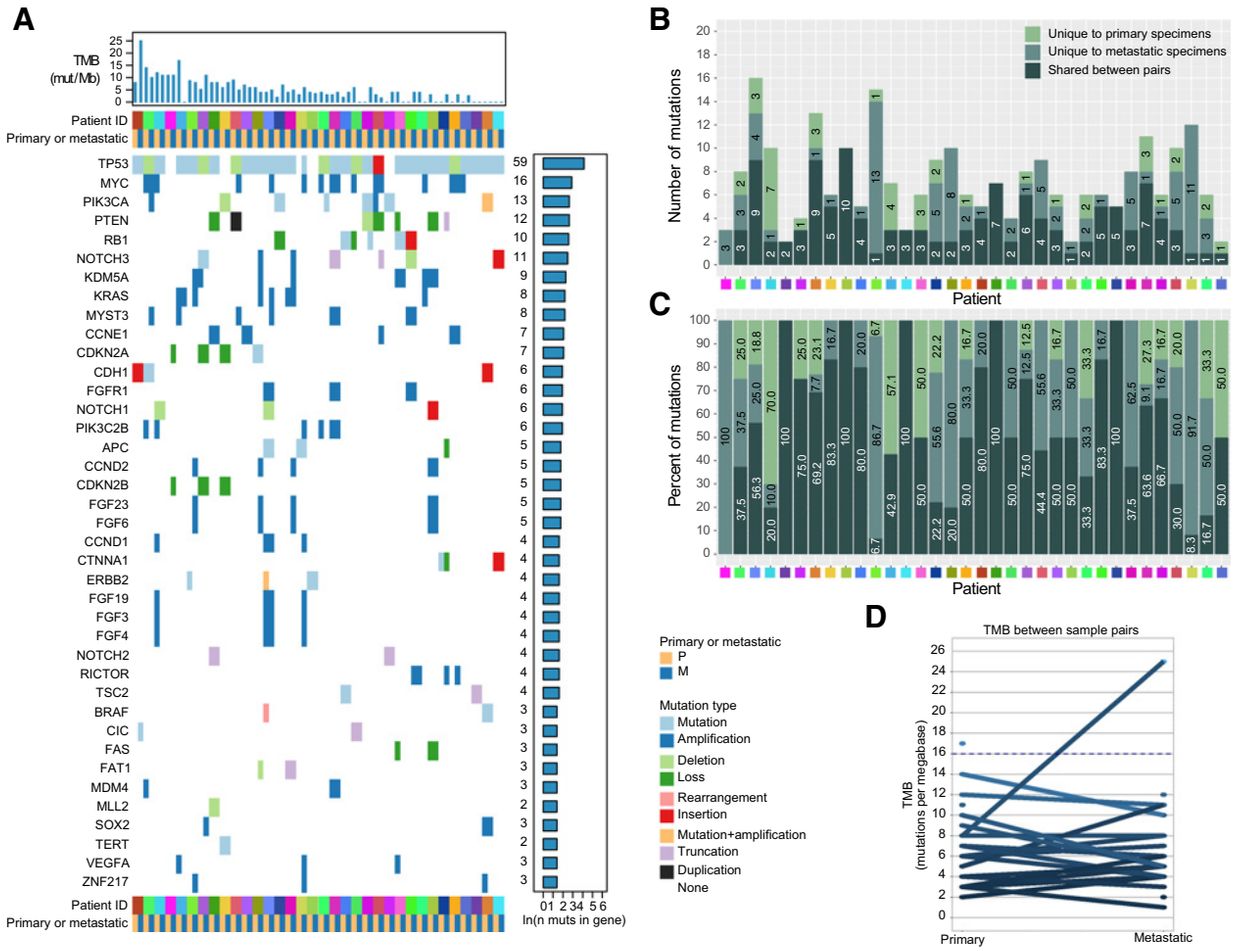

Figure 1.

Genomic landscape of PM TNBCs. FoundationOne targeted DNA sequencing was successfully performed on 34 PM TNBC pairs. **A,** The mutational landscape of these tumors was typical of TNBCs and similar between pairs. This figure displays data from patients who had a PM pair of specimens [i.e., no met-met (MM) specimens], and only known or likely oncogenic variants are shown (VUSs are not included). (**B**) Number and (**C**) percent of known or likely oncogenic variants unique to primary specimens, unique to metastatic specimens, or shared between pairs. **D,** Of the 34 PM TNBC pairs, 21 pairs yielded TMB results. With the exception of one primary sample and one metastatic sample (from different pairs), TMB was low/intermediate (<16 mutations per megabase) overall and relatively unchanged between TNBC pairs.

observed a downward shift in tumors characterized as BLIA (42.2% to 17.2%), with a concomitant increase in those characterized as BLIS (42.2% to 62.1%; **Fig. 2B**). Together, these data suggest that TNBCs become less immunologically rich over time.

TILs and survival

A number of prior TNBC studies have shown that stromal TIL levels exhibit a prognostic association with outcome in patients receiving adjuvant or neoadjuvant chemotherapy (27, 36, 37, 39, 40). We observed a modest, yet statistically significant decrease in the percentage of stromal TILs in primary versus recurrent specimens ($P = 0.02$, unpaired Mann–Whitney U test; **Fig. 3A**). Of 37 patients for which stromal TILs could be scored for both these patients' paired primary and metastatic specimens, 21 (56.8%) patients' tumor pairs displayed a decrease in stromal TILs in their metastatic disease specimens; 8 (21.6%) patients' tumor pairs displayed an increase in stromal TILs in metastatic disease; and 8 (21.6%) patients' tumor pairs exhibited no change in stromal TILs (**Fig. 3B**). Despite the PM pairs for which TILs either increased or did not change, the paired statistical analysis still revealed a statistically significant overall decrease in TILs in this population ($P = 0.03$, paired Student t test, **Fig. 3B**). No significant differences were observed when TILs were further subanalyzed by line of treatment (data not shown). These data are consistent with our analysis of TNBC molecular subtypes, above.

Using a cutoff of < 30% stromal TILs for "TIL-low" and ≥30% stromal TILs for "TIL-high" in this cohort (38), we analyzed TIL levels in relation to OS and SAR. For OS analysis, TILs scored in primary tumors were used; for SAR analysis, TILs scored in recurrent tumors were used. In this dataset, no significant difference in OS or SAR was observed at the defined 30% stromal TILs cut-off point (**Fig. 3C** and **D**).

Finally, although difficult to make any statistical inferences due to subgrouping of an already limited sample size, we observed a correlative trend of elevated stromal TILs with the IM, BLIA, and Basal-like breast cancer molecular subtypes as defined by the Lehmann/

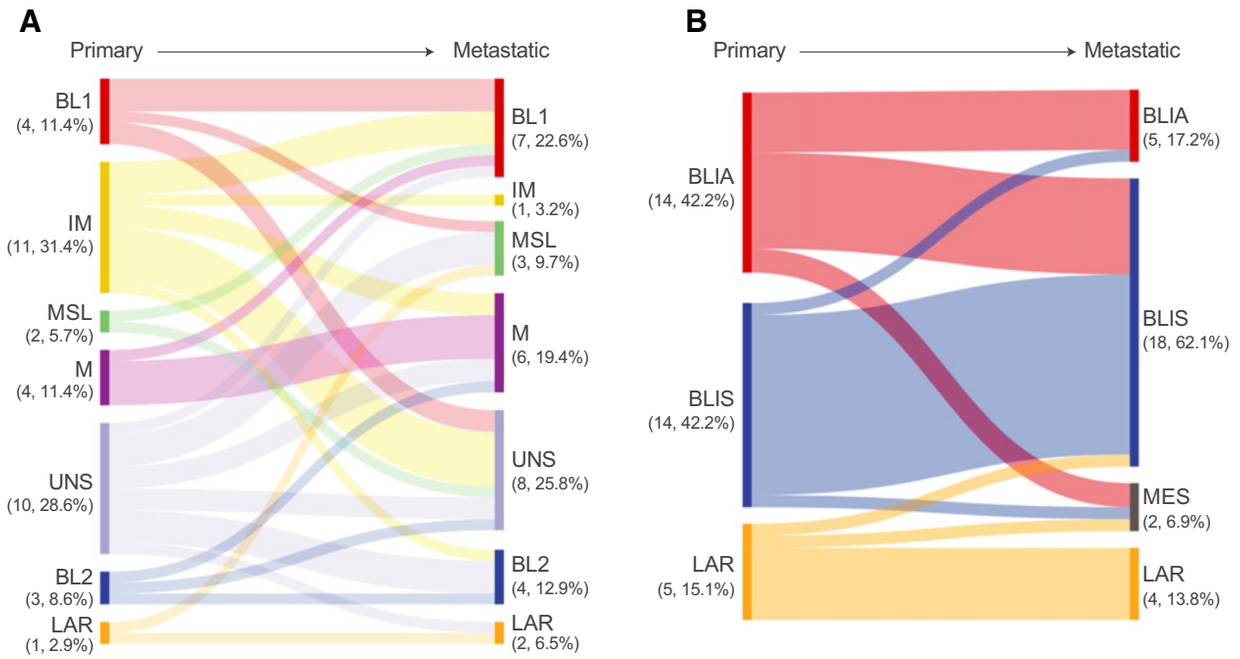

Figure 2.

Breast cancer molecular subtype shifts between primary and metastatic TNBC pairs. **A,** Classification of TNBC pairs into Lehmann/Pietenpol defined subtypes revealed an increase in the BL1 phenotype (11.4% to 22.6%), an increase in the mesenchymal phenotype (11.4% to 19.4%), and a significant decrease in the IM phenotype (31.4% to 3.2%). UNS, unspecified. **B,** Burstein-defined classifications revealed a decrease in the BLIA phenotype (42.2% to 17.2%), a converse decrease in the BLIS phenotype (42.2% to 62.1%), and an increase in the MES phenotype (0% to 6.9%). These analyses were performed on specimens from patients with PM pairs and of those, specimens for which a breast cancer subtype score were able to be assigned. Please note percentages may not add exactly to 100% due to rounding.

Pietenpol, Burstein, and PAM50 classifications, respectively (Supplementary Fig. S3B–S3D).

Differential gene expression analysis

RNA-seq was successfully performed on 35 PM pairs of specimens from the study cohort (Supplementary Fig. S1) upon which we employed a series of downstream analyses to understand gene expression as it relates to disease state, survival, and adjuvant/neoadjuvant therapy. First, comparing gene expression between primary and metastatic disease, significantly up- and downregulated differentially expressed genes were assessed for KEGG pathway (**Fig. 4A** and **B**; Supplementary Fig. S4A and S4B) and GO term (**Fig. 4C** and **D**; Supplementary Fig. S4C and S4D) enrichment. A clear enrichment of immune-related KEGG pathways was found among genes that were downregulated in metastatic samples compared with primary samples (**Fig. 4B**; Supplementary Fig. S4B). These included cytokine–cytokine receptor interactions, Th1 and Th2 cell differentiation, Th17 cell differentiation, natural killer cell–mediated cytotoxicity, T- and B-cell receptor signaling, and NFKB signaling. Interestingly, many of these pathways were also enriched among genes lending to HR < 1 in the Cox proportional hazards modeling for the OS, SAR, and TBC comparisons for primary (but not for metastatic) samples (see Materials and Methods; Supplementary Fig. S4B). We observed similar findings in the comparison between primary and metastatic samples through a ranked GSEA (Supplementary Fig. S4E–S4H).

Next, gene expression was analyzed separately in primary and metastatic samples using Cox proportional hazards regression modeling to understand whether expression of particular genes was associated with impacts to response variables, including OS, RFS, SAR, and TBC. A number of immune-related GO terms were enriched among downregulated genes in metastatic compared with primary samples, and among genes with HR < 1 in the OS, SAR, and TBC comparisons (**Fig. 4D**; Supplementary Fig. S4D). These included T-cell aggregation, B-cell receptor signaling, immune response activation, and the adaptive immune response. Together, these data indicate that genes comprising these KEGG pathway and GO terms are expressed at lower levels in metastatic versus primary TNBC samples, and increased expression of these genes in primary samples is associated with longer survival times. Other KEGG pathway and GO term comparisons were less thematic when contextualized with our broader data. Among upregulated genes, one KEGG pathway (spliceosome) was commonly enriched in the following comparisons: gene expression in metastatic versus primary specimens, gene expression in primary specimens versus RFS time, gene expression in metastatic specimens versus RFS time, and gene expression in primary specimens versus TBC (**Fig. 4A**; Supplementary Fig. S4A). Also among upregulated genes, GO terms associated with cellular cross-talk including cell–cell adhesion, extracellular exosomes, and extracellular organelles were enriched in the following comparisons: gene expression in metastatic versus primary specimens, gene expression in primary specimens versus RFS time, and gene expression in primary specimens versus TBC (**Fig. 4C**; Supplementary Fig. S4C).

Finally, to compare gene expression in patients as it relates to adjuvant/neoadjuvant therapy received, we performed differential gene expression in primary and metastatic samples comparing between the following categories of adjuvant/neoadjuvant therapy: adriamycin-containing (adriamycin cyclophosphamide, AC; cyclophosphamide adriamycin 5-FU, CAF; docetaxel adriamycin

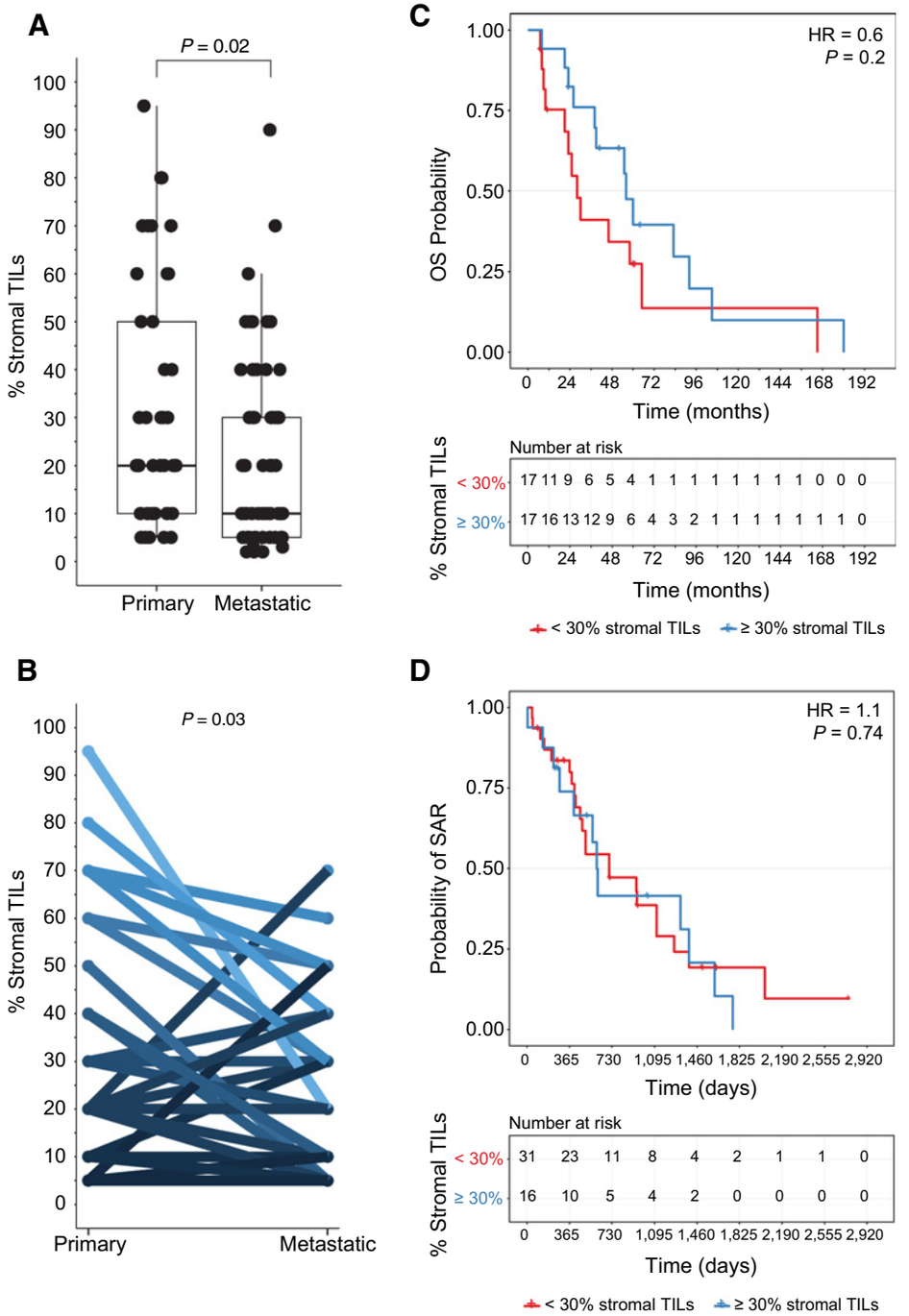

Figure 3.

TILs and survival. **A,** Histopathology-derived percent stromal TILs were significantly decreased in mTNBCs [$P = 0.02$, unpaired Mann–Whitney U (MWU) test]. **B,** Plotting only paired PM specimens longitudinally, whereas TILs are overall significantly decreased ($P = 0.03$, paired Student t test), some primary-to-metastatic pairs exhibited increases in stromal TILs in metastatic disease. **C,** Higher stromal TILs (≥30%) were not associated with improved OS when measured in primary specimens ($P = 0.2$), or (**D**) with the time from relapse to death when measured in recurrent specimens ($P = 0.74$). See Materials and Methods section for statistical considerations.

cyclophosphamide, TAC; or adriamycin cyclophosphamide paclitaxel, AC-T), platinum-containing (carboplatin paclitaxel), adriamycin and platinum-containing (adriamycin cyclophosphamide-carboplatin paclitaxel), taxane-containing (docetaxel cyclophosphamide, TC), or no adjuvant/neoadjuvant therapy. Gene expression in primary specimens from patients who received Adriamycin+platinum-containing regimens versus those who received adriamycin-containing therapies (without a platinum-based agent), taxane-containing therapies, or no adjuvant/neoadjuvant therapy revealed the only notable significant associations with specific KEGG pathways or GO terms. Specifically, the KEGG pathway "microRNAs in cancer" was enriched among upregulated genes as determined from primary specimens in the three adjuvant/neoadjuvant regimen comparisons above (Supplementary Fig. S4A). The GO terms extracellular exosome, extracellular organelles, and vesicles were enriched among significantly downregulated genes in these comparisons (Supplementary Fig. S4D). No notable associations were observed in adjuvant/neoadjuvant therapy comparisons using gene expression from metastatic samples.

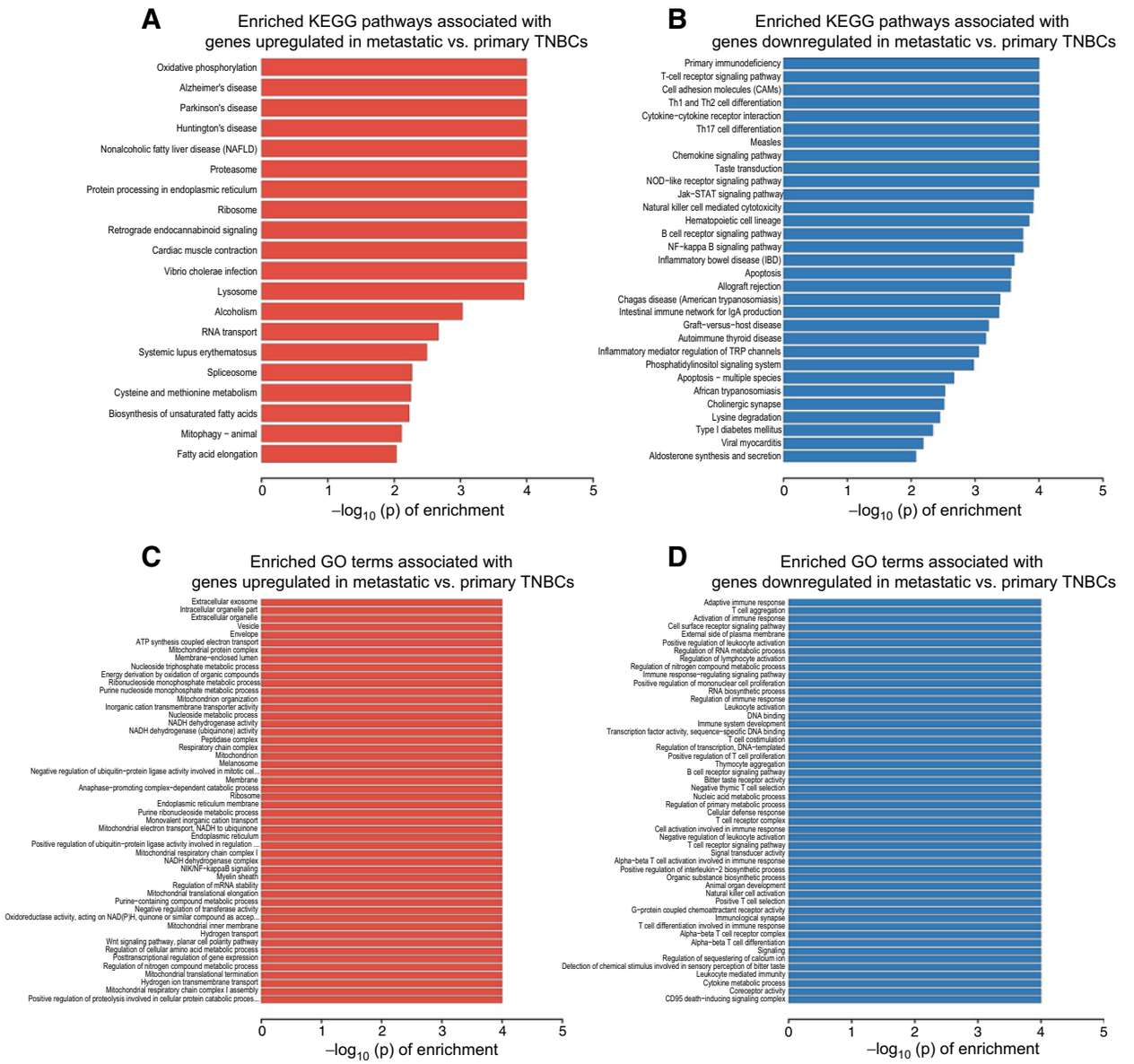

Figure 4.

KEGG pathway and GO term enrichment between primary and metastatic TNBC. KEGG pathway enrichment analysis associated with genes with (**A**) upregulated expression or (**B**) downregulated expression in metastatic compared with primary TNBCs revealed a clear enrichment of immune-related KEGG pathways among genes that were significantly downregulated in the metastatic samples. GO term enrichment analysis associated with genes with (**C**) upregulated expression or (**D**) downregulated expression in metastatic versus primary TNBCs revealed enrichment of a number of immune-related GO terms among downregulated genes in metastatic specimens. Bar plots herein display the pathway/term enrichment scores with $P < 0.01$. If more than 50 pathways/terms were significantly enriched, only the top 50 pathways are displayed for visualization purposes.

Immune phenotyping analysis of paired primary and mTNBCs

Considering the findings from the differential gene expression analyses above revealed a strong association of significantly downregulated genes in mTNBCs with immune-related KEGG pathways and GO terms, we further profiled the RNA-seq data from our cohort of specimens against four published gene signatures (lists) associated with immunologically active phenotypes: a 14-gene Th1 response–activating score, an 18-gene T-cell inflamed score, a 28-gene IFNγ score, and a 7-gene immune-activating score (36–38, 40, 41). Refer to the Materials and Methods for details on scoring and Supplementary Table S1 for the genes that comprise each signature. Composite intensity scores from three of the four gene signatures were significantly downregulated in metastatic samples compared with primary samples [**Fig. 5A** (heatmap) and **5B–E** (boxplots)]. Not surprisingly, we observed a concomitant trending decrease in the immune-related gene signature scores by line of therapy (Supplementary Fig. S5A–S5D) and positive correlation of each of these scores with percent stromal TILs (Supplementary Fig. S6A–S6D).

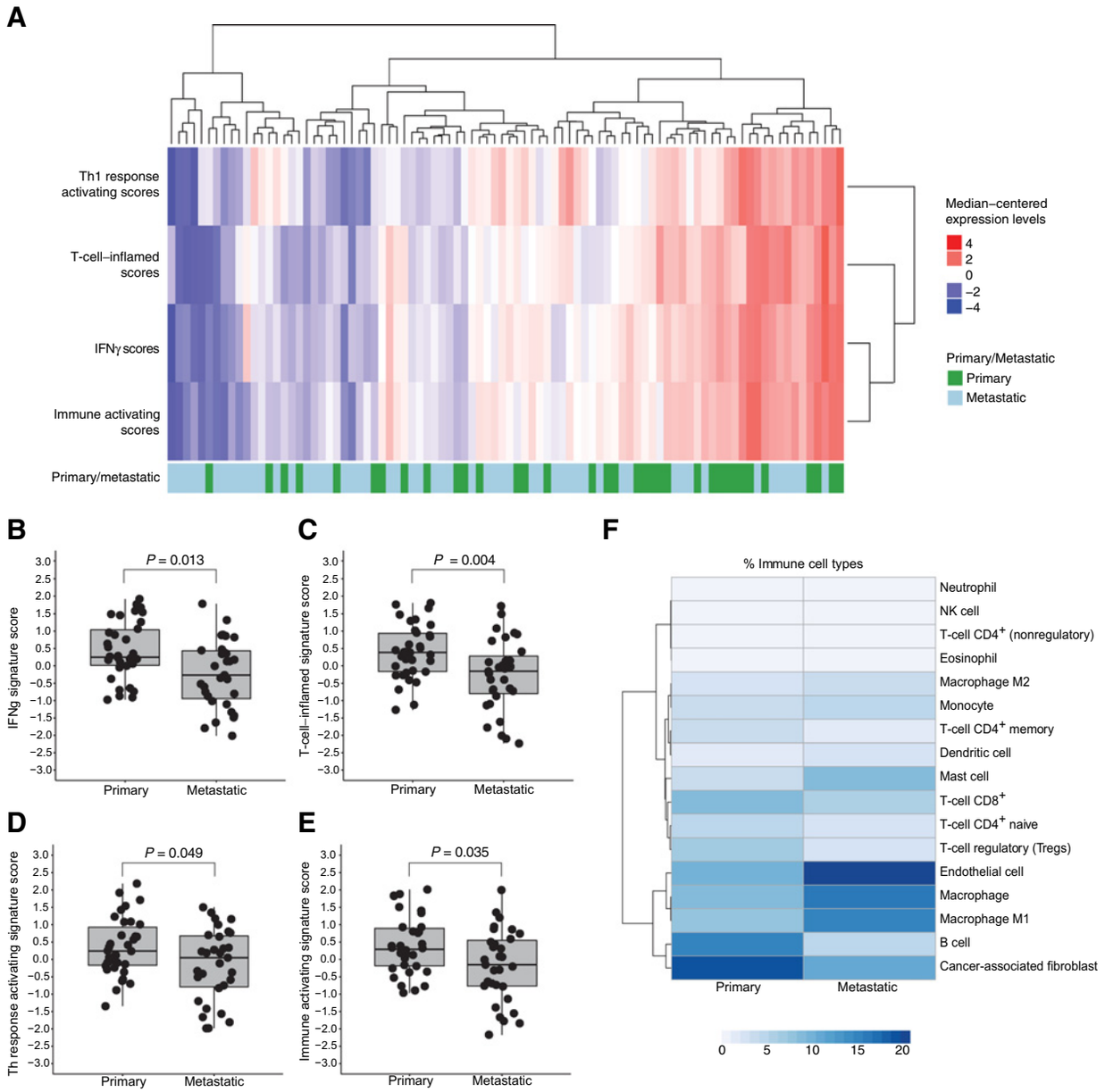

Figure 5.

Immune phenotype profiling between TNBC pairs. **A,** Heatmap of composite expression scores of immunomodulatory gene signatures between PM TNBC specimens. **B–E,** Boxplots of the same, to illustrate decreases in immunomodulatory gene signature scores between PM TNBC samples. Statistical analyses between primary and metastatic specimens were performed using the Mann–Whitney *U* test (unpaired), and *P* values < 0.05 were considered significant. **F,** Cell subtype proportions were summarized across primary and metastatic samples and depicted as an average percentage in the heatmap. Differences in proportions between the primary and metastatic groups were tested using a Wilcoxon signed rank test for each cell subtype, with *P* values adjusted for multiple test inflation using Benjamini–Hochberg correction. *P* values are presented in Supplementary Table S2.

To further understand possible shifts in immune-related cell subtypes, we estimated cell subtypes on paired primary and metastatic specimens for which RNA-seq was successful using the xCell immune cell deconvolution analysis (see Materials and Methods). The fraction of cell subtypes averaged across primary samples, and the fraction of cell subtypes averaged across metastatic samples, is summarized in **Fig. 5F**. Consistent with the immune-related gene signature phenotyping, in the transition from primary to metastatic disease, we observed significant decreases in the proportions of B-cell, $CD4^+$ naive T-cell, $CD8^+$ T-cell, and cancer-associated fibroblast subtypes. Conversely, we observed significant increases in the proportions of endothelial cell, macrophage, and M1 macrophage subtypes. A heatmap of the fraction of cell subtype for individual samples can be found in Supplementary Fig. S5E, and *P* values of the averaged fractions can be found in Supplementary Table S2.

Discussion

Molecular evolution of TNBC through chemotherapy selection pressure and the impact of this evolution toward next therapeutic steps are well recognized but poorly understood. In this study, we described the molecular changes observed in the largest paired primary-mTNBC cohort reported to date. We observed few mutational shifts and overall low TMB suggesting that tumors from patients treated with chemotherapies tend to maintain their genomic profiles over the course of therapy. We did, however, observe consistent transcriptomic shifts in longitudinally paired TNBCs. Transcriptomic and IHC analyses revealed significantly reduced expression of immune activity–associated gene expression signatures and of TILs in recurrent TNBCs. These data support the hypothesis that mTNBCs are less immunogenic compared with primary TNBCs and explain the lack of efficacy of ICIs in heavily pretreated patients in early clinical trials.

To better understand the molecular heterogeneity of TNBCs, several molecular classifiers have been developed [i.e., Lehmann/Pietenpol (8) and Burstein (9)]. Although helpful for our understanding of TNBC tumor biology, these molecular classifiers have little impact in guiding clinical practice. Previous studies comparing primary and metastatic breast cancers have provided variable results (41). Some studies indicated concordant overall expression patterns between primary breast cancers and their matched lymph nodes (42–45). Other studies identified discordant overall gene expression patterns between primary tumor and synchronous metastases (46). Weigelt and colleagues studied seven cases of primary breast cancer and asynchronous distant metastases and showed that a 70-gene prognostic signature (Mammaprint) was generally maintained in the switch from primary to metastasis across most of the pairs (47). As we attempted herein, some studies have used targeted NGS to address genomic concordance between primary and metastatic disease. For example, and confirming our findings, Meric-Bernstam and colleagues reported that 86.6% of the somatic mutations and 62.3% of the copy-number variations were concordant between primary tumors and recurrences (16). These studies highlight the limitation of tumor biopsies in capturing the heterogeneity of TNBC genomics and indicate the necessity of using alternative approaches for a more comprehensive understanding of the mutational spectrum of TNBCs (48). Furthermore, noncoding RNAs and epigenetic modifications may also play an important role in the metastatic process (42, 49, 50).

With recent FDA approval, ICI therapy is now a reality for patients with TNBC. As such, defining the appropriate population for such therapy is imperative. Atezolizumab increased PFS from 5.5 months to 7.2 months when added to a nab-paclitaxel as first-line treatment of patients with PD-L1–positive mTNBC (2, 19). In I-SPY2, more than 60% of patients with early-stage TNBC treated with neoadjuvant ACT (adriamycin, cyclophosphamide and paclitaxel) + pembrolizumab achieved a pCR, whereas patients who received chemotherapy alone only achieved an approximately 20% pCR rate (21). In heavily pretreated patients, however, response rates to single-agent ICIs decrease significantly. In cohort A of KEYNOTE-086 (PD-L1 agnostic cohort), 43.5% of patients with $\geq$ 3 lines of prior therapy achieved a response rate of 5.3% (18), suggesting that PD-L1 positivity is less of a response predictor in heavily pretreated patients. In contrast, in the PD-L1–positive cohort B of KEYNOTE-086, an overall response rate of 23% was observed in the first-line setting (17). Similarly, single-agent atezolizumab elicited a response rate of 24% (5 of 21) in patients with first-line mTNBC but only 5% (6 of 94) in patients with second-line or greater disease (19). These clinical trial data demonstrate that early intervention with immune checkpoint inhibition is associated with enhanced efficacy. Our study confirmed that metastatic breast cancers are immunologically more inert than their corresponding primary tumor, which is consistent with a recently published study by Szekely and colleagues (41). Our study provides a possible mechanistic explanation for clinical observations and further supports early incorporation of immune checkpoint blockade for patients with TNBC in the adjuvant/neoadjuvant setting.

This study is limited by its sample size, retrospective nature, and data in a cohort of patients not treated with immunotherapy. The sample size also precludes the ability to perform a subset analysis of the association of TIL levels and immune signature scores with sites of metastasis. Furthermore, our study's observed longitudinal genomic "similarities" could be a limitation of targeted exome sequencing which is unable to capture the entirety of genomic changes and epigenomic variations.

Disclosure of Potential Conflicts of Interest

R.M. Johnson, A.R. Carr, P.R. McAdam, D.L. Halligan, and J. Liang are employees/paid consultants for Genentech. Y. Yuan is a paid consultant for Genentech, Novartis, Puma, ImmunoMedics, and AstraZeneca, reports receiving commercial research grants from Genentech, Pfizer, Novartis, Eisai, and Puma, and speakers bureau honoraria from Novartis, AstraZeneca, Genentech, and Eisai. No potential conflicts of interest were disclosed by the other authors.

Authors' Contributions

Conception and design: K.E. Hutchinson, Y. Yuan
Development of methodology: K.E. Hutchinson, Y. Yuan
Acquisition of data (provided animals, acquired and managed patients, provided facilities, etc.): K.E. Hutchinson, S.E. Yost, Y. Yuan
Analysis and interpretation of data (e.g., statistical analysis, biostatistics, computational analysis): K.E. Hutchinson, S.E. Yost, C.-W. Chang, R.M. Johnson, A. Carr, P. McAdam, D.L. Halligan, C.-C. Chang, D. Schmolze, Y. Yuan
Writing, review, and/or revision of the manuscript: K.E. Hutchinson, S.E. Yost, C.-W. Chang, R.M. Johnson, D. Schmolze, J. Liang, Y. Yuan
Administrative, technical, or material support (i.e., reporting or organizing data, constructing databases): K.E. Hutchinson, S.E. Yost, J. Liang, Y. Yuan
Study supervision: K.E. Hutchinson, J. Liang, Y. Yuan

Acknowledgments

The authors would like to thank the following teams, individuals, and additional funding sources: colleagues Dhara Shah and Craig Cummings in Genentech's Oncology Biomarker Development (OBD) Data Science group for performing post–RNA-seq data processing and normalization; colleagues Sophia Maund, also in the OBD Data Science group at Genentech, and Ethan Sokol from Foundation Medicine, Inc., for providing expert input regarding technical aspects of Foundation Medicine testing; the STOP Cancer Foundation for their support of principal investigator Y. Yuan. Y. Yuan, MD, PhD is also supported through an NCI K-12 Career Development Award (K12CA001727, principal investigator: Joanne Mortimer) and the NIH (P30CA033572). Research reported in this publication included work performed in the Pathology Research Services Core, Biostatistics and Mathematical Modeling Core, Integrative Genomics Core, and Bioinformatics Core supported by the NCI of the NIH under award number P30CA033572. The content is solely the responsibility of the authors and does not necessarily represent the official views of the NIH.

The costs of publication of this article were defrayed in part by the payment of page charges. This article must therefore be hereby marked *advertisement* in accordance with 18 U.S.C. Section 1734 solely to indicate this fact.

Received May 30, 2019; revised August 7, 2019; accepted October 9, 2019; published first October 14, 2019.

References

1. Plasilova ML, Hayse B, Killelea BK, Horowitz NR, Chagpar AB, Lannin DR. Features of triple-negative breast cancer: analysis of 38,813 cases from the national cancer database. Medicine 2016;95:e4614.
2. Schmid P, Adams S, Rugo HS, Schneeweiss A, Barrios CH, Iwata H, et al. Atezolizumab and nab-paclitaxel in advanced triple-negative breast cancer. N Engl J Med 2018;379:2108–21.
3. Robson ME, Im S-A, Senkus E, Xu B, Domchek SM, Masuda N, et al. OlympiAD: phase III trial of olaparib monotherapy versus chemotherapy for patients (pts) with HER2-negative metastatic breast cancer (mBC) and a germline BRCA mutation (gBRCAm). J Clin Oncol 2017;35:18s, (suppl; abstr LBA4).
4. Litton JK, Rugo HS, Ettl J, Hurvitz SA, Gonçalves A, Lee K-H, et al. Talazoparib in patients with advanced breast cancer and a germline BRCA mutation. N Engl J Med 2018;379:753–63.
5. Anders CK, Carey LA. Biology, metastatic patterns, and treatment of patients with triple-negative breast cancer. Clin Breast Cancer 2009;9:S73–S81.
6. The Cancer Genome Atlas Network. Comprehensive molecular portraits of human breast tumours. Nature 2012;490:61.
7. Lehmann BD, Pietenpol JA. Clinical implications of molecular heterogeneity in triple negative breast cancer. Breast 2015;24Suppl 2:S36–40.
8. Lehmann BD, Bauer JA, Chen X, Sanders ME, Chakravarthy AB, Shyr Y, et al. Identification of human triple-negative breast cancer subtypes and preclinical models for selection of targeted therapies. J Clin Invest 2011;121:2750–67.
9. Burstein MD, Tsimelzon A, Poage GM, Covington KR, Contreras A, Fuqua SA, et al. Comprehensive genomic analysis identifies novel subtypes and targets of triple-negative breast cancer. Clin Cancer Res 2015;21:1688–98.
10. Lehmann BD, Jovanović B, Chen X, Estrada MV, Johnson KN, Shyr Y, et al. Refinement of triple-negative breast cancer molecular subtypes: implications for neoadjuvant chemotherapy selection. PLoS One 2016;11:e0157368.
11. Almendro V, Kim HJ, Cheng Y-K, Gönen M, Itzkovitz S, Argani P, et al. Genetic and phenotypic diversity in breast tumor metastases. Cancer Res 2014;74:1338–48.
12. Park SY, Gönen M, Kim HJ, Michor F, Polyak K. Cellular and genetic diversity in the progression of *in situ* human breast carcinomas to an invasive phenotype. J Clin Invest 2010;120:636–44.
13. Wang Y, Waters J, Leung ML, Unruh A, Roh W, Shi X, et al. Clonal evolution in breast cancer revealed by single nucleus genome sequencing. Nature 2014;512:155.
14. Curtis C, Shah SP, Chin SF, Turashvili G, Rueda OM, Dunning MJ, et al. The genomic and transcriptomic architecture of 2,000 breast tumours reveals novel subgroups. Nature 2012;486:346–52.
15. The Cancer Genome Atlas Network. Comprehensive molecular portraits of human breast tumours. Nature 2012;490:61–70.
16. Meric-Bernstam F, Frampton GM, Ferrer-Lozano J, Yelensky R, Perez-Fidalgo JA, Wang Y, et al. Concordance of genomic alterations between primary and recurrent breast cancer. Mol Cancer Ther 2014;13:1382–9.
17. Adams S, Schmid P, Rugo HS, Winer EP, Loirat D, Awada A, et al. Pembrolizumab monotherapy for previously treated metastatic triple-negative breast cancer: cohort A of the phase II KEYNOTE-086 study. Ann Oncol 2018 Nov 26;30:397–404.
18. Adams S, Schmid P, Rugo HS, Winer EP, Loirat D, Awada A, et al. Phase 2 study of pembrolizumab (pembro) monotherapy for previously treated metastatic triple-negative breast cancer (mTNBC): KEYNOTE-086 cohort A. J Clin Oncol 2017;35:15s.
19. Emens LA, Cruz C, Eder JP, Braiteh F, Chung C, Tolaney SM, et al. Long-term clinical outcomes and biomarker analyses of atezolizumab therapy for patients with metastatic triple-negative breast cancer: a phase 1 study. JAMA Oncol 2019;5:74–82.
20. Nanda R, Chow LQ, Dees EC, Berger R, Gupta S, Geva R, et al. Pembrolizumab in patients with advanced triple-negative breast cancer: phase Ib KEYNOTE-012 study. J Clin Oncol 2016;34:2460–7.
21. Nanda R, Liu MC, Yau C, Asare S, Hylton N, Veer LVt, et al. Pembrolizumab plus standard neoadjuvant therapy for high-risk breast cancer (BC): results from I-SPY 2. J Clin Oncol 2017;35:15s(suppl; abstr 506).
22. Salgado R, Denkert C, Demaria S, Sirtaine N, Klauschen F, Pruneri G, et al. The evaluation of tumor-infiltrating lymphocytes (TILs) in breast cancer: recommendations by an International TILs Working Group 2014. Ann Oncol 2015;26:259–71.
23. Sergushichev A. An algorithm for fast preranked gene set enrichment analysis using cumulative statistic calculation. BioRxiv2016.
24. Parker JS, Mullins M, Cheang MC, Leung S, Voduc D, Vickery T, et al. Supervised risk predictor of breast cancer based on intrinsic subtypes. J Clin Oncol 2009;27:1160–7.
25. Perou CM, Parker JS, Prat A, Ellis MJ, Bernard PS. Clinical implementation of the intrinsic subtypes of breast cancer. Lancet Oncol 2010;11:718–9.
26. Perou CM, Sorlie T, Eisen MB, van de Rijn M, Jeffrey SS, Rees CA, et al. Molecular portraits of human breast tumours. Nature 2000;406:747–52.
27. Denkert C, von Minckwitz G, Brase JC, Sinn BV, Gade S, Kronenwett R, et al. Tumor-infiltrating lymphocytes and response to neoadjuvant chemotherapy with or without carboplatin in human epidermal growth factor receptor 2-positive and triple-negative primary breast cancers. J Clin Oncol 2015;33:983–91.
28. Ayers M, Lunceford J, Nebozhyn M, Murphy E, Loboda A, Kaufman DR, et al. IFN-gamma-related mRNA profile predicts clinical response to PD-1 blockade. J Clin Invest 2017;127:2930–40.
29. Chtanova T, Newton R, Liu SM, Weininger L, Young TR, Silva DG, et al. Identification of T cell-restricted genes, and signatures for different T cell responses, using a comprehensive collection of microarray datasets. J Immunol 2005;175:7837–47.
30. Chtanova T, Tangye SG, Newton R, Frank N, Hodge MR, Rolph MS, et al. T follicular helper cells express a distinctive transcriptional profile, reflecting their role as non-Th1/Th2 effector cells that provide help for B cells. J Immunol 2004;173:68–78.
31. Grotz TE, Jakub JW, Mansfield AS, Goldenstein R, Enninga EA, Nevala WK, et al. Evidence of Th2 polarization of the sentinel lymph node (SLN) in melanoma. Oncoimmunology 2015;4:e1026504.
32. Aran D, Hu Z, Butte AJ. xCell: digitally portraying the tissue cellular heterogeneity landscape. Genome Biol 2017;18:220.
33. Sturm G, Finotello F, Petitprez F, Zhang JD, Baumbach J, Fridman WH, et al. Comprehensive evaluation of transcriptome-based cell-type quantification methods for immuno-oncology. Bioinformatics 2019;35:i436–i45.
34. Giltnane JM, Hutchinson KE, Stricker TP, Formisano L, Young CD, Estrada MV, et al. Genomic profiling of ER(+) breast cancers after short-term estrogen suppression reveals alterations associated with endocrine resistance. Sci Transl Med 2017;9:pii:eaai7993.
35. Kwek SS, Roy R, Zhou H, Climent J, Martinez-Climent JA, Fridlyand J, et al. Co-amplified genes at 8p12 and 11q13 in breast tumors cooperate with two major pathways in oncogenesis. Oncogene 2009;28:1892–903.
36. Loi S, Michiels S, Salgado R, Sirtaine N, Jose V, Fumagalli D, et al. Tumor infiltrating lymphocytes are prognostic in triple negative breast cancer and predictive for trastuzumab benefit in early breast cancer: results from the FinHER trial. Ann Oncol 2014;25:1544–50.
37. West NR, Milne K, Truong PT, Macpherson N, Nelson BH, Watson PH. Tumor-infiltrating lymphocytes predict response to anthracycline-based chemotherapy in estrogen receptor-negative breast cancer. Breast Cancer Res 2011;13:R126.
38. Ohtani H, Mori-Shiraishi K, Nakajima M, Ueki H. Defining lymphocyte-predominant breast cancer by the proportion of lymphocyte-rich stroma and its significance in routine histopathological diagnosis. Pathol Int 2015;65:644–51.
39. Denkert C, von Minckwitz G, Darb-Esfahani S, Lederer B, Heppner BI, Weber KE, et al. Tumour-infiltrating lymphocytes and prognosis in different subtypes of breast cancer: a pooled analysis of 3771 patients treated with neoadjuvant therapy. Lancet Oncol 2018;19:40–50.
40. Dieci MV, Criscitiello C, Goubar A, Viale G, Conte P, Guarneri V, et al. Prognostic value of tumor-infiltrating lymphocytes on residual disease after primary chemotherapy for triple-negative breast cancer: a retrospective multicenter study. Ann Oncol 2014;25:611–8.
41. Szekely B, Bossuyt V, Li X, Wali V, Patwardhan G, Frederick C, et al. Immunological differences between primary and metastatic breast cancer. Ann Oncol 2018;29:2232–9.
42. Krøigård AB, Larsen MJ, Thomassen M, Kruse TA. Molecular concordance between primary breast cancer and matched metastases. Breast J 2016;22:420–30.
43. Ellsworth RE, Seebach J, Field LA, Heckman C, Kane J, Hooke JA, et al. A gene expression signature that defines breast cancer metastases. Clin Exp Metastasis 2009;26:205–13.
44. Suzuki M, Tarin D. Gene expression profiling of human lymph node metastases and matched primary breast carcinomas: clinical implications. Mol Oncol 2007;1:172–80.

45. Hao X, Sun B, Hu L, Lähdesmäki H, Dunmire V, Feng Y, et al. Differential gene and protein expression in primary breast malignancies and their lymph node metastases as revealed by combined cDNA microarray and tissue microarray analysis. Cancer 2004;100:1110–22.
46. Vecchi M, Confalonieri S, Nuciforo P, Vigano M, Capra M, Bianchi M, et al. Breast cancer metastases are molecularly distinct from their primary tumors. Oncogene 2008;27:2148.
47. Weigelt B, Hu Z, He X, Livasy C, Carey LA, Ewend MG, et al. Molecular portraits and 70-gene prognosis signature are preserved throughout the metastatic process of breast cancer. Cancer Res 2005;65:9155–8.
48. Rothe F, Laes JF, Lambrechts D, Smeets D, Vincent D, Maetens M, et al. Plasma circulating tumor DNA as an alternative to metastatic biopsies for mutational analysis in breast cancer. Ann Oncol 2014;25:1959–65.
49. Gravgaard KH, Lyng MB, Laenkholm AV, Søkilde R, Nielsen BS, Litman T, et al. The miRNA-200 family and miRNA-9 exhibit differential expression in primary versus corresponding metastatic tissue in breast cancer. Breast Cancer Res Treat 2012;134:207–17.
50. Chisholm KM, Wan Y, Li R, Montgomery KD, Chang HY, West RB. Detection of long non-coding RNA in archival tissue: correlation with polycomb protein expression in primary and metastatic breast carcinoma. PLoS One 2012;7:e47998.